JTTEE5 16:978–990
DOI: 10.1007/s11666-007-9130-8
1059-9630/$19.00 © ASM International

Flame-Sprayed Glaze Coatings: Effects of Operating Parameters and Feedstock Characteristics Onto Coating Structures

A. Arcondéguy, A. Grimaud, A. Denoirjean, G. Gasgnier, C. Huguet, B. Pateyron, and G. Montavon

(Submitted April 4, 2007; in revised form September 8, 2007)

Many substrates do not sustain the conventional glazing process (i.e., vitreous glazing) due to the relatively high temperature required by this treatment (i.e., up to 1400 °C in some cases) to fuse glazes after their application on the surface to be covered. Flame spraying could appear as a solution to circumvent this limitation and to avoid thermal decomposition of substrates. This contribution describes some structural attributes of glaze coatings manufactured by flame spraying. It also discusses the influence of the feedstock powder morphology and some of its physical properties on coating characteristics.

Keywords feedstock architecture, feedstock composition, flame spraying, glaze, operating parameters, thermally sensitive substrate, thick layer

1. Introduction

Glazing can be depicted as coating a substrate by fusing various mineral substances over it. Glazes can be applied onto metallic or ceramic substrates. Therefore, they find numerous applications, from art ornamenting to protection against corrosion, thanks to their design characteristics (i.e., colors, brightness, opacity, etc.) and physical properties (i.e., low thermal conductivity, tightness, etc.). This process, known since ancient times, needs a relatively high temperature treatment (i.e., from 500 °C to up to 1400 °C in some cases) that some substrates do not sustain. For this reason, developing a glaze-deposition technique by thermal spraying may appear interesting as it could prevent, or at least limit, the substrate material from thermal degradation.

Glazes are mainly made up of silica and alumina, which are refractory materials (i.e., high melting points). Furthermore, these ceramics present a relatively low viscosity when molten, which can affect the coating formation compared to spraying of more conventional ceramic materials. Finally, glazes also exhibit lower thermal conductivity due to the relatively high fraction of silica. Some characteristics of alumina and silica (Ref 1, 2) are listed in Table 1. Glaze composition can be very complicated as many oxides can be added to adjust their physical properties, for example (by wt.%): 64.0 SiO_2, 15.0 B_2O_3, 7.6 Al_2O_3, 6.9 Na_2O, 2.9 BaO, 2.1 CaO, and 1.5 ZnO (Ref 3). With such complex composition, glaze properties are significantly different from pure silica and pure alumina (Ref 3).

Recent studies show that feedstock characteristics widely affect the coating morphology. For example, the powder morphology and particle size distribution had to be adjusted to spraying process when considering different thermal spray processes (atmospheric plasma spraying or high-velocity oxygen fuel spraying) for manufacturing bioactive glass ceramic (with a transition temperature of 610 °C) coatings on titanium alloys. As a consequence, spherical agglomerated powders (with average diameter of about 40 μm) are more adaptive than precipitated powders that exhibit very poor flowability (Ref 4).

Other works related to spray mullite coatings onto molybdenum sheets by low-pressure plasma spraying proved that an addition of glass (with a transition temperature of 610 °C) to mullite increased the coating porosity (from 3 to 12%), but reduced residual stresses (Ref 5). By adjusting the mullite/glass ratio, coefficient of thermal expansion (CTE) of the coating might approach that of the substrate (Ref 6). In other cases, such as coatings obtained by water-stabilized plasma spraying, open porosity of coatings can be modified by different annealings (Ref 7).

Furthermore, coating properties depend upon spray parameters: increasing power levels and spray distance lead to an increase in coating porosity and tensile strength (Ref 4). A study done on plasma spraying of borosilicate glass on steel substrates proved the existence of a coating

This article is an invited paper selected from presentations at the 2007 International Thermal Spray Conference and has been expanded from the original presentation. It is simultaneously published in *Global Coating Solutions, Proceedings of the 2007 International Thermal Spray Conference*, Beijing, China, May 14-16, 2007, Basil R. Marple, Margaret M. Hyland, Yuk-Chiu Lau, Chang-Jiu Li, Rogerio S. Lima, and Ghislain Montavon, Ed., ASM International, Materials Park, OH, 2007.

A. Arcondéguy, A. Grimaud, A. Denoirjean, B. Pateyron, and **G. Montavon**, SPCTS-UMR CNRS 6638, Faculty of Sciences, University of Limoges, 123 avenue Albert Thomas, 87060, Limoges cedex, France; and **G. Gasgnier** and **C. Huguet**, Imerys Tableware France, 1 rue Jeanne d'Albret, 87700, Aixe-sur-Vienne, France. Contact e-mail: ghislain.montavon@unilim.fr.

Table 1 Comparison of alumina and silica properties

	Unit	Alumina	Silica
Specific mass	g/cm^3	3.75-3.93	2.15-2.17
Kinematics viscosity	m^2/s	1.026×10^{-5}	...
Glass transition temperature	°C	...	1327–1427
Melting temperature	°C	2047-2057	1713
Maximal operating temperature	°C	1627-1827	877-1077
Specific heat	J/kg/K	780-850	690-780
Boiling temperature	°C	3530	2700
Thermal conductivity	W/m/K	24-35 @ 20 °C	1.2-1.6 @ 20 °C
		10-15 @ 500 °C	...
Heat transfer coefficient	10^6 W/K/m^2	8.0-8.9	0.52-0.65
Coefficient of thermal expansion (CTE)	10^{-6}/K	8-9	0.5-0.7

critical thickness related to the residual stress level: coating adhesion decreases when coating thickness increases due to residual stress increases. These results clearly mention that compressive residual stresses are less detrimental to coating quality than tensile residual stresses (Ref 8).

This article intends to present some developments carried out to process glaze feedstock by flame spraying to coat substrates sensitive to thermal degradation. At first, the selection of the deposition process (i.e., powder flame spraying) is presented and a brief economical benchmark is detailed. Then, the thermal flux transferred from the flame to the substrate is quantified as it modifies the substrate structure, when thermally sensitive, but also the coating structure and its properties. The effects of selected operating parameters (i.e., power parameters, geometrical parameters, kinematics, and environmental parameters) on coating structure for a given glaze composition are then presented. At last, the effect of the glaze characteristics, in terms of composition and morphology, are detailed.

2. Spray Process

2.1 Process Selection

In this study, the spray powder particles are melted within an oxyacetylene flame. Simultaneously, they get accelerated before their impact, flattening and solidification onto the substrate to form the coating. The flame results from an exothermic reaction between a fuel gas (acetylene) and a combustive-fuel gas (oxygen), which can be expressed at stoichiometry (i.e., stoichiometric coefficient $\phi = 1$) as follows:

$$C_2H_2 + \frac{5}{2}O_2 \rightarrow H_2O + 2CO_2 + \Delta H \quad \text{(Eq 1)}$$

where $\Delta H = -1300$ kJ/mol (Ref 9).

Most of the experiments were carried-out with $\phi = 0.6$ corresponding to the following reaction:

$$C_2H_2 + \frac{3}{2}O_2 \rightarrow x_1H_2O + x_2CO_2 + x_3CO + x_4C_2H_2 \quad \text{(Eq 2)}$$

where x_1, x_2, x_3, and x_4 represent stoichiometric coefficients.

Depending on the selected stoichiometry, the resulting maximal flame temperature varies between 2800 to 3100 °C, and hence agrees with the transition temperatures of common glazes. Furthermore, flame temperature is adapted to volatile materials like silica. This results from the lower enthalpy density of the flame (compared to the one of a plasma jet for example) and from the longer particle residence time within the flame due to a lower gas-flow velocity; this improves the softening of feedstock exhibiting low thermal conductivity (Ref 10).

2.2 Estimation of Operating Costs

This economic estimation is a preliminary study aiming mostly at estimating orders of operating costs considering several scenarios. They represent estimations as costs of supplies largely vary according to ordered quantities, countries, etc., and very significantly varies the labor cost depending on the country. In the following, neither pretreatment nor posttreatment costs were considered (coating is directly applied onto the thermally sensitive substrate) and the costs are estimated for a production line operating 35 h a week, 355 days a year (maintenance operations being carried out at night).

Calculation considers at first, one flame torch in operation and a surface to be covered by one square meter. Coating characteristics and data from suppliers are displayed in Table 2. These data permit to estimate the deposited coating mass according to its thickness, taking into account deposition efficiencies varying between 50 and 70% (common values for this type of feedstock sprayed implementing a not-fully optimized process). From deposition rates, the deposition duration to reach a given thickness can be deduced too. From these results, abacuses are built to represent relationships between coating thickness, coating mass, required mass of feedstock, and deposition duration (Fig. 1). Labor cost is proportional to deposition duration too. One considers that only one technician is required for operating the spray system. Furthermore, investments are necessary to launch the production (Table 2): it consists in the manufacturing of a dedicated production line equipped at first with one flame torch and one powder feeder. Amortization is estimated on a basis of 5 years: this means that it is also a function of the deposition duration.

To roughly estimate the total cost for one piece of one square meter, one just has to add the contributions of supplies, labor, and investments. With such a simplified approach, the total cost goes from 10.53 €/m^2 (with

Table 2 Suppliers data used for calculating the operating costs

Coating characteristics	Thickness, mm	From 0.20 to 0.30		
	Porosity, vol.%	5		
Glaze property	Density, g/cm^3	2.5		
Flame spraying characteristics	Deposition efficiency, %	From 50 to 70		
	Deposition rate, kg/h	About 3		
Supplies	Gas	Composition	Flow, NL/h	Cost, 0.01 €/L
		O_2	2000	0.10
		C_2H_2	1800	0.34
	Glaze	Cost, €/kg	1.5	
Equipment	Flame torch		Unit price, €	Service life, h
		Nozzle	200	100
			Power, kW	kWh cost, €
		Energy consumption	28 (supplier data)	0.11
Labor (technician)	Salary, €/h	17.60 (average value, in France in 2007)		
Investment (five-year amortization)	Flame torch, €	7000 (average cost)		
	Powder feeder, €	25,000		
	Kinematics (special device), €	200,000		

Costs are expressed in €; they have to be multiplied by 1.3, average value, to express them in US $

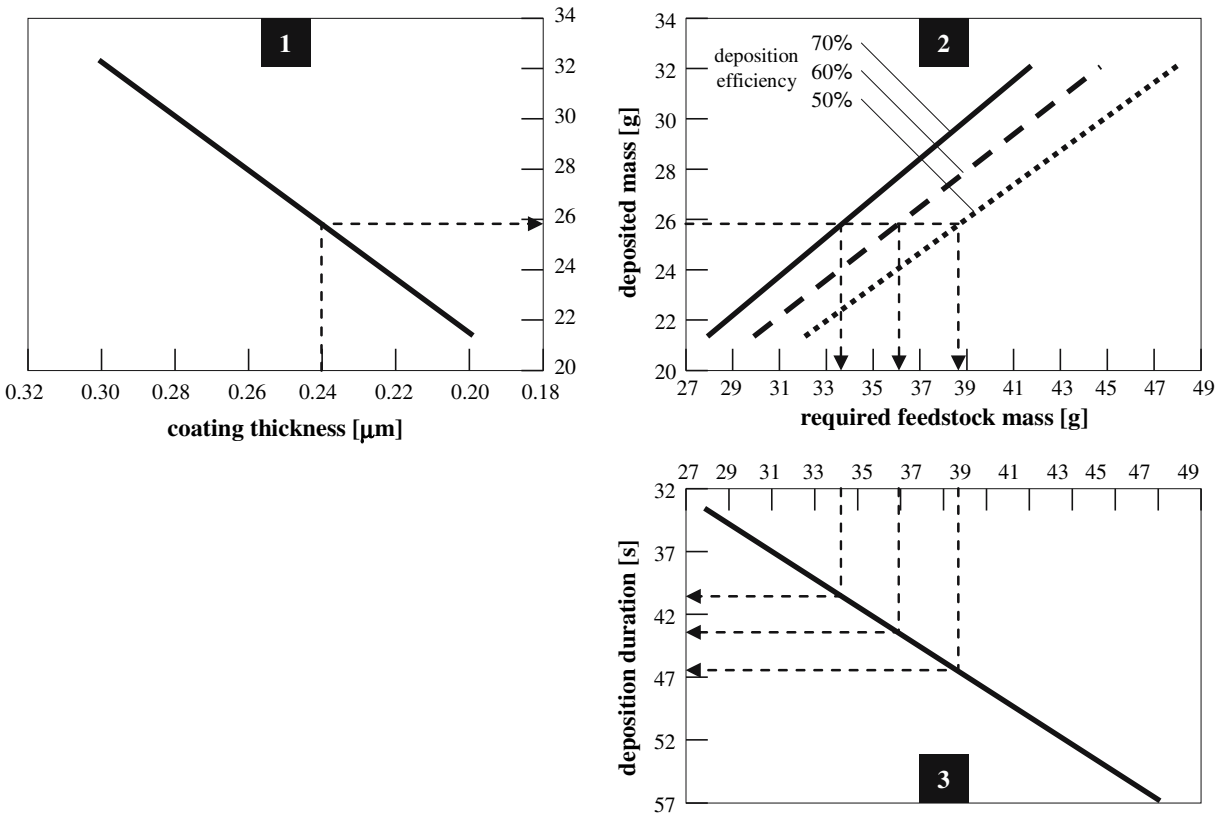

Fig. 1 Relationships between the coating thickness, deposited mass, required feedstock mass, and deposition duration for a surface of one square meter

a thickness of 0.20 mm and a deposition rate of 70%) to 18.23 €/m^2 (with a thickness of 0.30 mm and a deposition rate of 50%). All of the results are detailed in Table 3. Supplies have the highest contribution in the total cost.

This total cost can be decreased by increasing the number of flame torches operating at the same time on the same machine controlled by the same operator. As a consequence, when considering, for example, 4 torches, the cost per square meter is reduced by a third (mostly due to the decrease in the labor cost). With such a configuration, the total cost varies from 7.60 to 13.16 €/m^2. From an economic point of view, glaze and meanwhile this estimation of the costs would need to be adapted specific to

Table 3 Cost for one square meter, according to the coating thickness, the deposition rate and the torches number

Coating thickness, mm	Deposition efficiency, %	Cost for 1 m², €			
		1 torch	2 torches	3 torches	4 torches
0.20	50	12.15	9.90	9.15	8.77
	60	11.34	9.24	8.54	8.19
	70	10.53	8.58	7.93	7.60
0.25	50	15.19	12.37	11.44	10.97
	60	14.18	11.55	10.67	10.24
	70	13.17	10.72	9.91	9.50
0.30	50	18.23	14.85	13.72	13.16
	60	17.01	13.86	12.81	12.28
	70	15.80	12.87	11.89	11.40

Costs are expressed in €; they have to be multiplied by 1.3, average value, to express them in US $

each condition (including maintenance costs for example), spraying hence can be considered as a viable technique compared to traditional glazing and, in some cases, to painting.

3. Thermal Flux Measurements

Mechanisms occurring during glaze-coating manufacturing by flame spraying may differ from those usually encountered when considering more traditional materials such as oxides or even carbides. Indeed, the coating results from the coalescence of molten particles and is manufactured in one pass rather than the stacking of individual lamellae and several passes. It is therefore important to estimate the thermal flux transmitted from the torch to the substrate, as it has to be high enough to improve the particles spreading and wettability without, nevertheless, leading neither to thermal decomposition of the substrate nor to the development of unacceptable levels of residual stresses.

Heat flux measurements were carried out using water calorimeters made of copper circular bodies of different diameters (12, 20, 39, 58, 78, and 120 mm, respectively) and the backside is cooled down with a controlled water flow. Thermocouples measured the upstream and downstream water temperature evolution, as the copper bodies were exposed to the flame heat flux. Knowing the temperature differences and the water flow rates, one can calculate the heat quantity transferred by flame to calorimeter as follows:

$$Q = m_{\text{water}} \cdot C_{p_{\text{water}}} \left(T_{\text{upstream}} - T_{\text{downstream}}\right) \quad \text{(Eq 3)}$$

where Q is the transferred heat (J), m_{water} is the water mass (kg), $C_{p_{\text{water}}}$ is the water specific heat at constant pressure (4.18×10^3 J/kg per kelvin), and T_{upstream} and $T_{\text{downstream}}$ are the measured temperatures (K) at the entrance and the exit of the calorimeter, respectively.

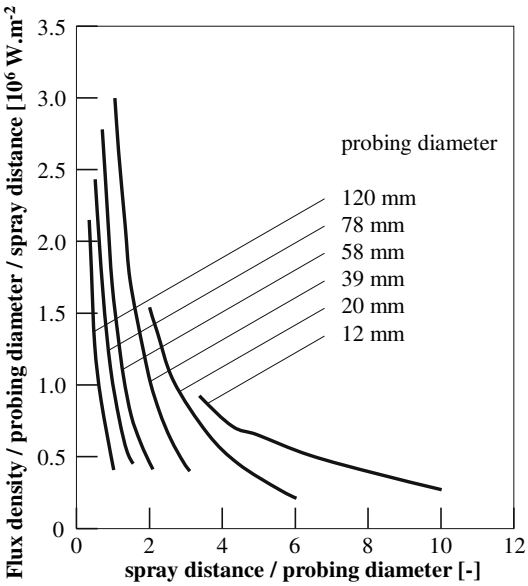

Fig. 2 Transferred flux to the substrate for different diameter surfaces depending on the spray distance

The equivalent transferred thermal power is then determined as follows:

$$P_{\text{th}} = \frac{dQ}{dt} = D_{\text{water}} \cdot d_{\text{water}} \cdot C_{p_{\text{water}}} \left(T_{\text{upstream}} - T_{\text{downstream}}\right) \quad \text{(Eq 4)}$$

where P_{th} is the transferred thermal power (W), Q is the transferred heat (J), t is the time (s), D_{water} is the measured water flow rate (m^3/s), d_{water} is the water specific mass at the considered temperature (kg/m^3), $C_{p_{\text{water}}}$ is the water specific heat at constant pressure (4.18×10^3 J/kg per kelvin), and T_{upstream} and $T_{\text{downstream}}$ are the measured temperatures (K) at the entrance and the exit of the calorimeter, respectively.

Finally, the thermal flux density (W/m^2) can be deduced as being the ratio of the thermal power P_{th} related to the measurement area (m^2).

Tests were realized in static configurations and Fig. 2 displays the evolution of the calculated corrected thermal flux density (flux density/probing diameter/spray distance) vs. corrected distance (spray distance/probing diameter). One can deduce that the flux is inversely proportional to the spray distance (following hyperbolic relationships). Flux density evolves from 0.3 to 3 MW/m^2 when the probing diameter is divided by ten. The maximal flux density results from a probing diameter of 58 mm and a ratio of a spray distance to the probing diameter ratio is less than 2.

Such an energy level will have to be high enough to maintain a semi-molten state of the glaze layer without being too high to thermally damage the substrate. A compromise is therefore to be determined concerning the spray distance.

4. Effects of Operating Parameters on Coating Structure

4.1 Glaze Characteristics

A first study was realized considering a glaze powder (made of alumina, silica and various other oxides aiming at adjusting the transition temperature, the viscosity, and the surface tension of the material when in the liquid state), denoted A, manufactured by agglomeration and sintering. This work indented to test 12 different glaze compositions. Composition A reflects a baseline composition from which adjustments were made in the second time. Quantification of its physical properties was carried out by thermo-gravimetric analysis consisting in measuring the relative mass variation of a sample over a thermal cycle. Experimental data then results from the comparison of the sample parameter evolutions to those of an inert reference. Analysis was realized with a Thermovac TM 20 (Oerlikon Leybold Vacuum GmbH, Köln, Germany) thermo-gravimetric apparatus under air at ambient pressure. The thermal cycle was defined according to the feedstock supplier specifications, which specifies, among other physical characteristics, a glaze transition temperature of about 1050 °C. The thermal cycle considered hence: a temperature increase from ambient to 900 °C at a heating rate of 10 °C/min, a plateau at the maximum temperature during 12 min and a temperature decrease from 900 °C to ambient at a cooling rate of 15 °C/min.

The measured data (Fig. 3) shows that there is nearly no significant mass loss when the temperature increases. This means that no chemical reaction occurs during thermal cycling. One can assume, nevertheless, that the very small mass loss (less than 0.1%) results from some organic binder evaporation added at the time of the glaze agglomeration and not fully vaporized during the sintering step.

4.2 Spray Parameters

Flame-spraying operating parameters can be divided into four groups: power parameters (for a given flame torch geometry, gas mixture, gas flow rates, mostly), geometrical parameters (spray distance, among others), kinetics parameters (spray torch velocity, scanning step among the principals), and environmental parameters (cooling for example). The primary objective of the first study was to estimate the major effects of several operating parameters on the structure of glaze coatings and to identify operating parameter windows.

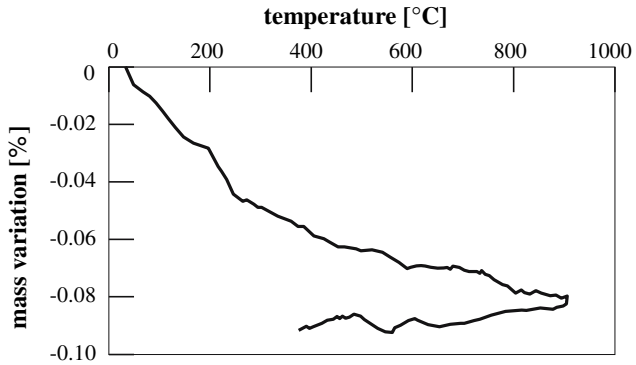

Fig. 3 Powder A relative mass loss vs. temperature

Coatings result from one pass in front of substrates ($40 \times 40 \times 15$ mm) made of a hydraulic binder whose composition and characteristics are confidential. Such substrates are thermally sensitive, a material bursting might occur at temperatures of about 250 or 300 °C (Ref 11). Furthermore, these substrates present a porous structure and exhibit low thermal conductivity, of about 2 W/mper kelvin (supplier data). Substrates were dried (24 h at 50 °C) before spraying, since water desorption needs absolutely to be avoided during flame spraying, but no surface preparation was considered. Table 4 displays the operating parameters that were considered in this study.

The flame torch used in this study is a DS 8000 (CastoDyn, Lausanne, Switzerland), operated with a mixture of oxygen and acetylene. The total gas flow rate was kept constant at 50 SLPM. Depending on the relative mass flow rates for oxygen and acetylene, flame stoichiometry varies from sub-stoichiometry (oxygen excess) to stoichiometry and over-stoichiometry (acetylene excess). Flame temperature evolves according to the stoichiometry and the maximum flame temperature is reached for a 0.7 stoichiometry. At first, a stoichiometry of 0.6 was considered (following the supplier recommendation and some previous tests). It corresponds to a commonly used value in flame spraying.

The variables were the spray distance (60 or 90 mm), the torch-substrate relative spray velocity (0.075 or 0.150 m/s), and the scanning step (4 or 9 mm). Torch position was fixed whereas substrates were moved simultaneously following two axes (translation, determining the scanning step, and rotation, determining the spray velocity, movement in front of torch by scanning step motors).

One can consider in a first approximation that decreasing the spray distance leads to a very significant decrease in the particles temperature (modifying the particle behavior during spreading) whereas the particles' velocity remains almost constant. Also, the particle footprint dimensions depend on the spray distance and the scanning step has to be adjusted accordingly. Moreover, this distance plays a relevant role on the heat flux transmitted from the source to the substrate.

Table 4 Considered operating spray parameters

Set #	Spray distance, mm	Scanning step, mm	Spray velocity, m/s
1	60	4	0.075
2	60	4	0.150
3	60	9	0.075
4	60	9	0.150
5	90	4	0.075
6	90	4	0.150
7	90	9	0.075
8	90	9	0.150

Flame stoichiometry is kept constant at 0.6

Spray velocity also plays a relevant role on the heat flux transmitted to the substrate: the lower the spray velocity, higher is the heat flux. Even if this can be a disadvantage, as it can lead to possible residual stresses within the coating, but can have beneficial effects as the particle wettability is improved, which is important when considering glazes.

4.3 Coating Structure

In thermal spraying, classical coatings result from molten spread particles stacking (discrete phenomena). For glazes, the coating manufacturing mechanisms are different. Indeed, because of the high surface tension, contact angle between the substrate and the molten particle is greater than 90°, which prevents the particle from being totally spread (i.e., ''dewetting'' phenomena). Coating results from coalescence of impinging particles to form a monolayer (Ref 12).

Coating thicknesses were statistically determined by image analysis on coating polished cross sections of SEM pictures for each coating (from six randomly located pictures along the cross sections). Table 5 displays the results.

The resulting coating thicknesses are significantly influenced by the operating parameters. These thicknesses can be typified as thick (thicknesses from 150 to 700 μm) with variability nearly constant and of small amplitude. As the spray distance decreases, the coating thickness decreases since both the particle temperature at impact and the thermal flux transferred by the source increase (Sets #1 and #4 in Table 4). As a result, the viscosity and surface tension of the glaze particles decrease and their spreading increased. From the same prospect, the overlapping is increased when decreasing the scanning step (Sets #2 and #3 in Table 4). The highest thickness results from Set # 5 corresponding to a layer with very high porosity.

Table 5 Effect of spray parameters on coating thickness

Set #	Spray distance, mm	Spray velocity, m/s	Scanning step, mm	Average thickness, μm	Variability, %
1	60	0.075	9	323	5
2	60	0.150	9	157	5
3	60	0.150	4	259	5
4	90	0.075	9	411	7
5	90	0.075	4	689	4

Figure 4(a) displays a typical upper surface morphology of an as-sprayed glaze layer. It is characterized by large globular pores distributed uniformly along the layer. The shape of the pores within the layer is explained by coalescence of the pores within the powder particles during the layer manufacturing since glaze stays in the mushy stage for a longer period of time. Nearly no crack is visible on the coating surfaces (the very few are probably caused by the cutting required for sample preparation).

In low energy conditions (Fig. 4b), the coating upper surface morphology presents globular porosity too but an ''orange peel''-like surface develops at the same time: this is very likely due to the presence of a significant number of small particles which do not travel within the flame due to turbulent dispersion, and do not possess enough momentum and heat, preventing the particles from spreading. They ultimately stick on the layer during its formation.

The substrate-coating interface was observed by SEM from fractured samples. There is no sign of apparent delamination at the interface in spite of the presence of globular pores (Fig. 5). Substrates did not suffer from heat

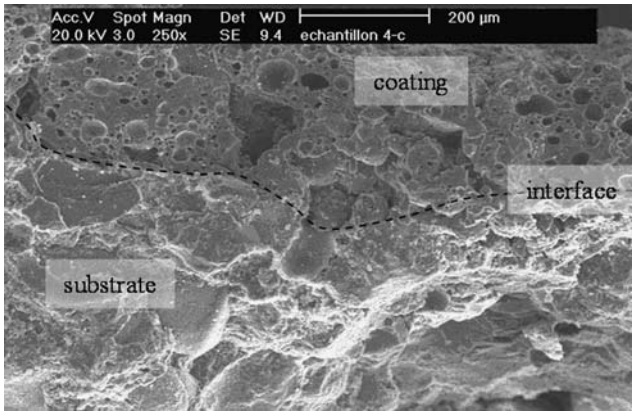

Fig. 5 Substrate-coating interface microstructure (SEM-SE) (×250 magnification)

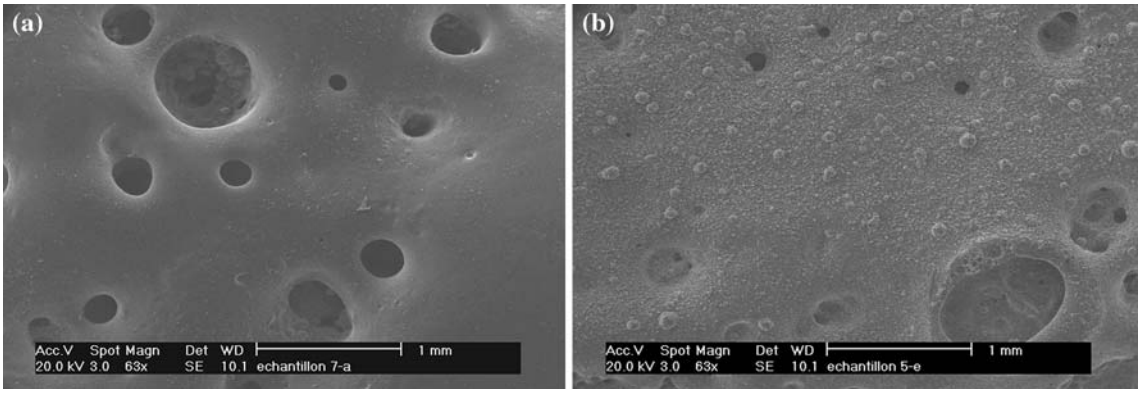

Fig. 4 Morphology of coating surface (SE-SEM) obtained with (a) high and (b) low energy parameters

Table 6 Tested glaze powders

		Calculated transition temperature, °C, from Lengersdorff model	Calculated surface tension, N/m, from Dietzel model	Calculated coefficient of linear expansion, 10^{-7}/°C, from Happen model
Agglomerated-sintered powders	Powder A	1050	364×10^{-3}	64
	Powder B	850	283×10^{-3}	88
Fused-crushed powders	Powder X	850	n.a.	n.a.
	Powder Y	800	n.a.	n.a.
	Powder Z	560	n.a.	n.a.

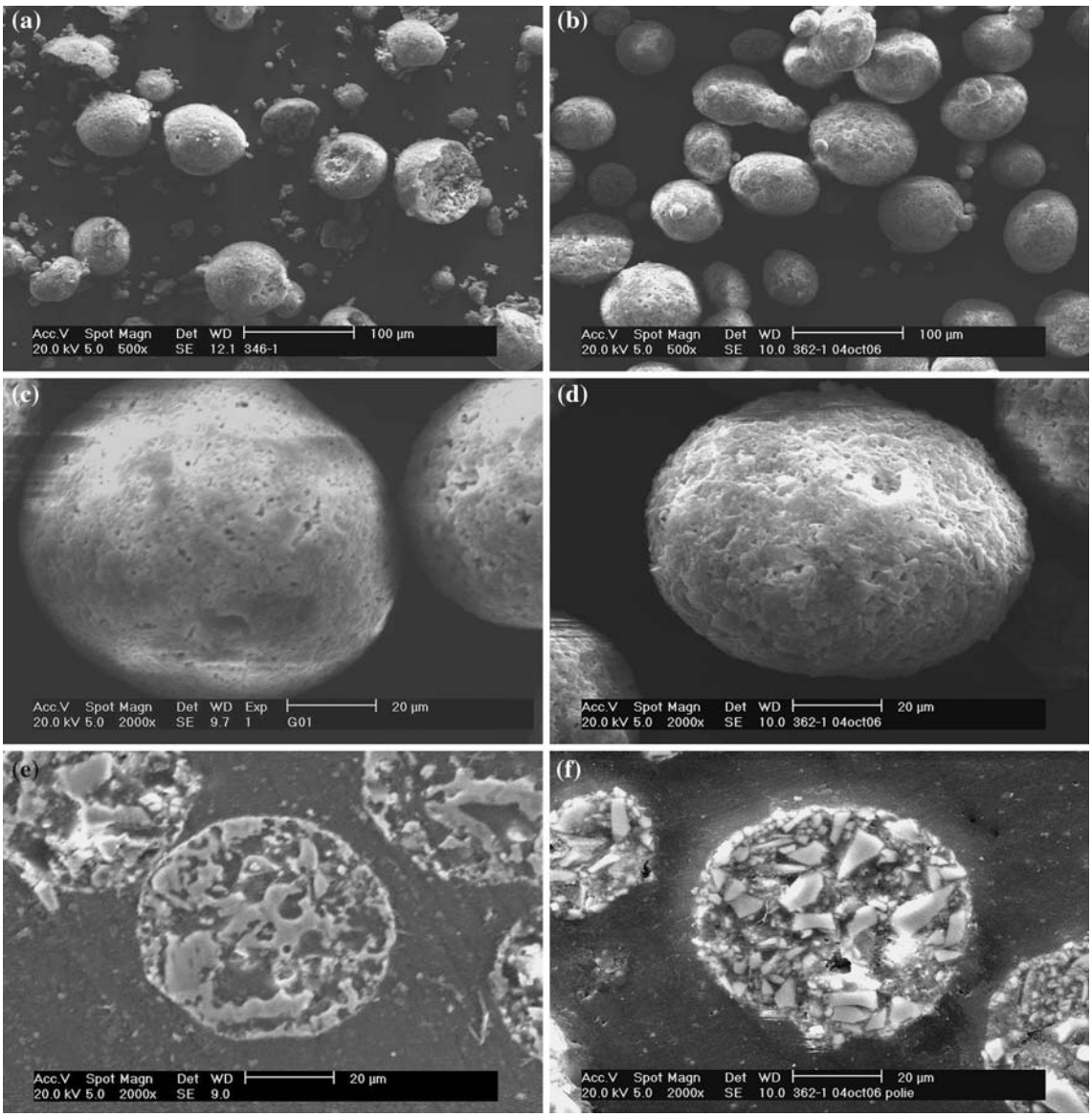

Fig. 6 Morphology (SE-SEM) of glaze powders formed by atomization. (a) As-received powder A (×500 magnification). (b) As-received powder B (×500 magnification). (c) As-received powder A (×2000 magnification). (d) As-received powder B (×2000 magnification). (e) Polished cross section of powder A (×2000 magnification). (f) Polished cross section of powder B (×2000 magnification)

treatment, as transferred heat measurements and calculation of substrate temperature during spraying tend to confirm. Additional structural and chemical analyses are underway to further confirm this point.

From these results, set # 6 was selected as ''reference'' spray parameters and were used later on to test and compare different glazes powders of different morphologies and compositions. Of course, spray parameters will

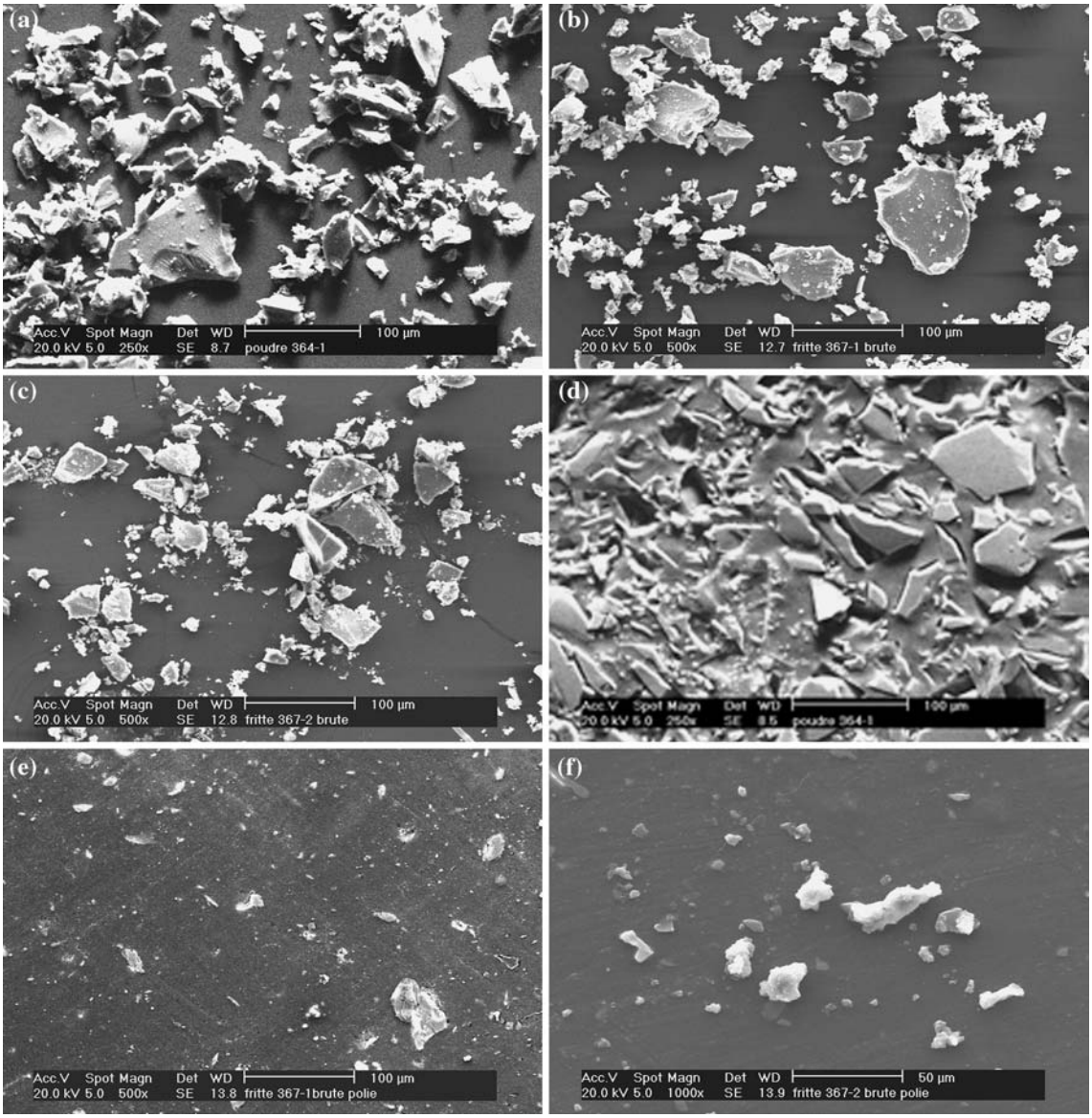

Fig. 7 Morphology (SE-SEM) of glaze powders formed by crushing (×500 magnification). (a) As-received powder X. (b) As-received powder Y. (c) As-received powder Z. (d) Polished cross section of powder X. (e) Polished cross section of powder Y. (f) Polished cross section of powder Z

have to be even more optimized depending on the glaze composition.

5. Effects of Feedstock Characteristics on Coating Structure

5.1 Feedstock Characteristics

This second study aimed at optimizing morphology and thermal properties of feedstock powder. For constant spray parameters displayed in Table 4, glazes of various chemical compositions, corresponding to different transition temperatures, ranging from 560 to 1050 °C, and of various morphologies, corresponding to different manufacturing processes (agglomeration-sintering, agglomeration-sintering and flame densification, fusing and crushing), were tested. These glazes are mainly made up of alumina, silica and other oxides (fluxes) to adjust glaze transition temperature, viscosity, and surface tension (detailed chemical compositions of these glazes specifically manufactured are confidential). Some calculated characteristics of the considered powders are detailed in Table 6.

Feedstock morphologies were observed using a Philips XL 30 (Koninklijke Philips Electronics N.V., Eindhoven, The Netherlands). SEM (Scanning Electron Microscopy) is operated in the secondary electron (SE) mode.

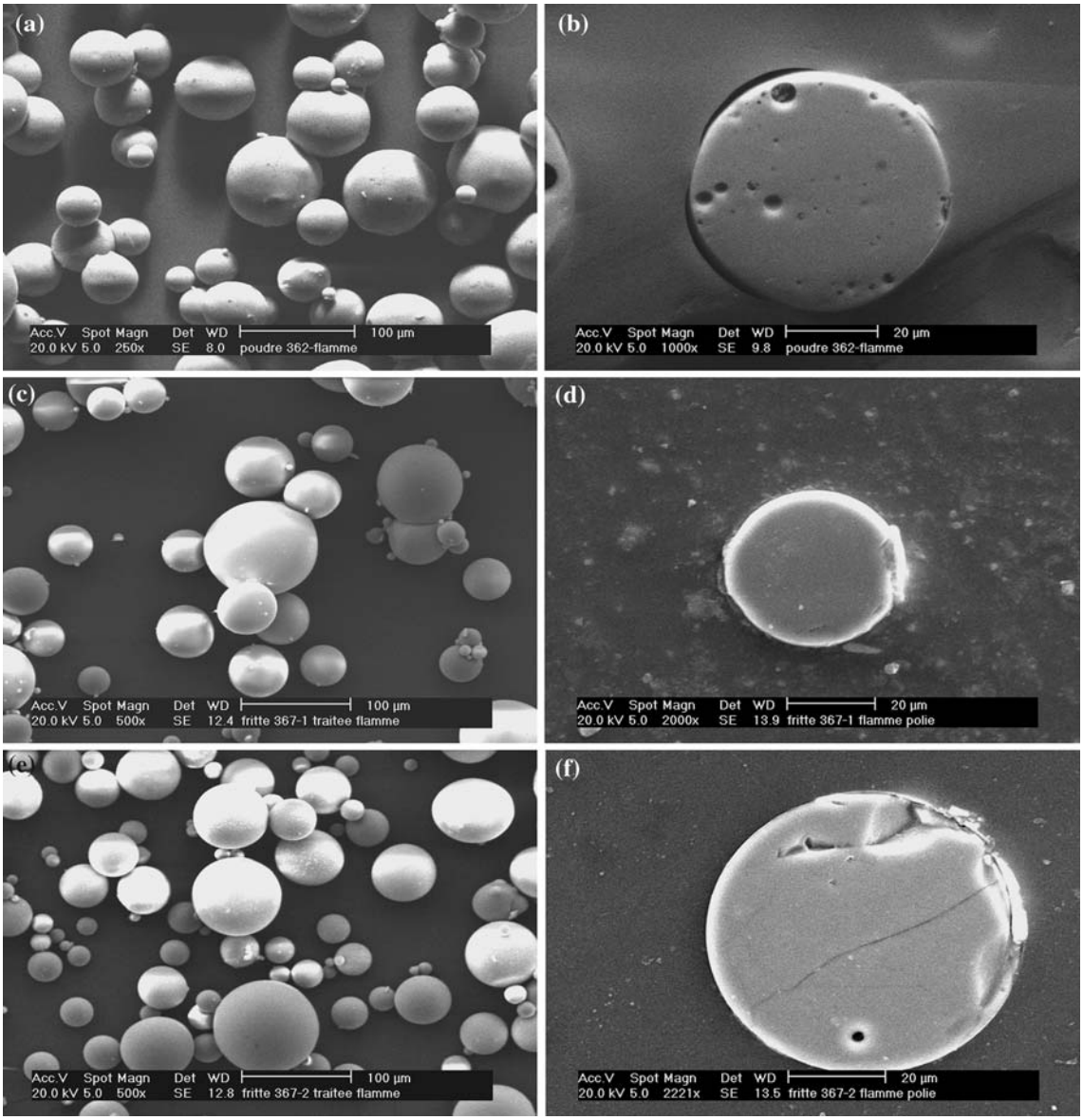

Fig. 8 Morphology (SE-SEM) of the polished cross section of glazes processed by flame treatment. (a) As-received powder B (×500 magnification). (b) Polished cross section of powder B (×2000 magnification). (c) As-received powder Y (×500 magnification). (d) Polished cross section of powder Y (×2000 magnification). (e) As-received powder Z (×500 magnification). (f) Polished cross-section powder Z (×2000 magnification)

The spherical morphology (Fig. 6a, b) is very typical from the agglomeration-sintering process that was implemented to manufacture feedstock A and B. Nevertheless, an apparent open porosity is clearly discernable (Fig. 6c, d) and is a representative of pores within powder particles. Figure 6(e) and (f) displays the cross section of the as-received feedstock and clearly highlights its porous character. In a first approximation, one can estimate that the porosity level is about 20%. Such a level is fairly high. Furthermore, those pores seem to be highly connected.

On the contrary, feedstock powders X, Y, and Z are made of dense angular particles of irregular shapes (Fig. 7) typical of the fusing and crushing process. These powders present broad particle-size distributions too, with very fine particles (Fig. 7a-c). The angular morphology coupled to the broad particle size distribution renders the feedstock flowability, especially poor.

To reduce the particle porosity (for powders A and B) and render them spherical (powders X, Y, and Z), they were processed by flame treatment and collected in water. After decantation, feedstock were dried. Figure 8 shows that this treatment is efficient because the particles morphology is considerably modified, as expected.

A laser particle size analyzer was used to quantify the particle size distribution after flame treatment. This technique is based on light diffraction (i.e., Fraunhofer

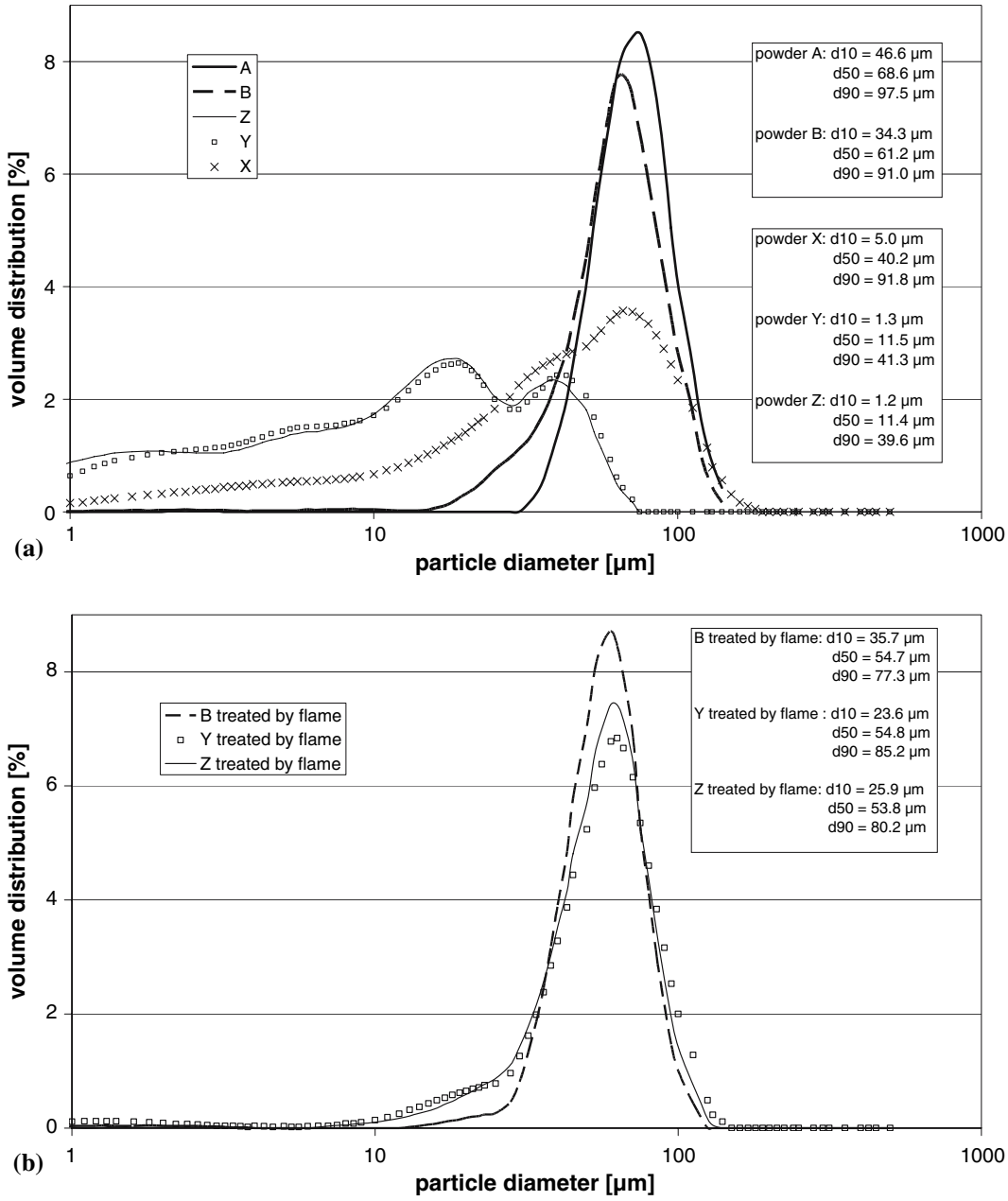

Fig. 9 Particle volume size distribution of (a) as-manufactured powders and (b) powders treated by flame

theory). Measurements were carried out in the dry mode implementing a Cilas 1064 laser analyzer (Cilas, Orléans, France).

As displayed in Fig. 9(a), glaze powders A and B exhibit a monomodal particle size distribution, nearly Gaussian, centered around 70 µm (d_{50}), contrary to powders X, Y, and Z, which present particle size distributions that can be typified as bimodal with a peak centered around 35, 19, and 18 µm and a second one centered around 68, 37, and 38 µm, respectively. Such values are consistent with SEM observations.

Nevertheless, for as-received powders A and B, more than 50% of the number of particles exhibits an average diameter smaller than 1 µm. Very likely, those very fine particles result from the fragmentation of larger ones during their interaction with the flame due to an incomplete sintering. Concerning as-received powders X, Y, and Z, only 40%, average value, of particles present an average diameter lower than 1 µm: it might be explained by an agglomeration of fine particles caused by the milling.

After flame treatment, particle size distributions are modified and are all monomodal, centered around 55 µm (d_{50}) (Fig. 9b), whatever the as-received powder. For example, d_{50} of powder B decreases from 65 to 55 µm. This volume reduction is due to their densification when processed through the flame. Furthermore, the greater

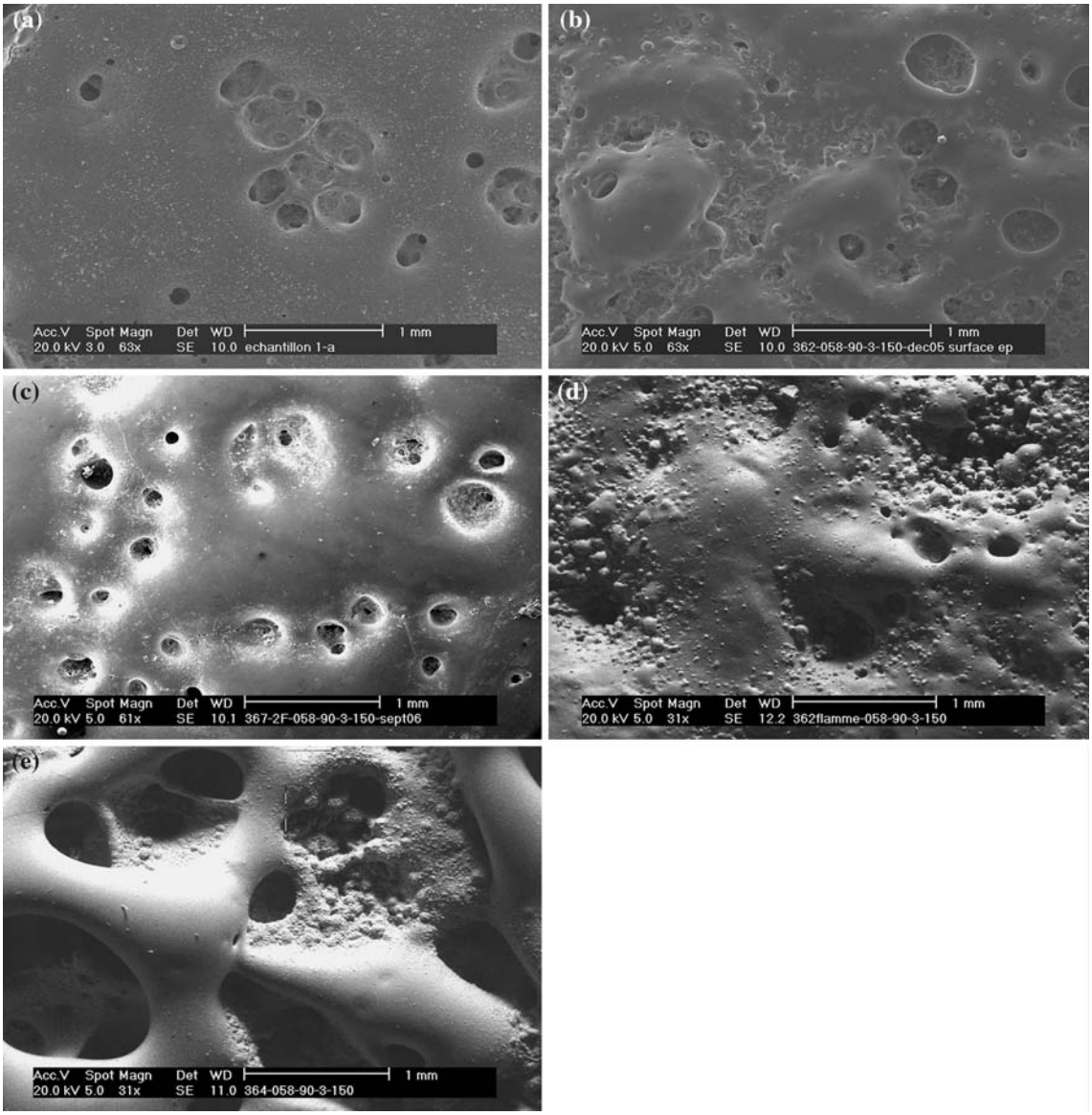

Fig. 10 Microstructure (SE-SEM) of a coating surface (×63 magnification) obtained with (a) powder A, (b) powder B, (c) powder Z, (d) powder B treated by flame, and (e) powder X

part of fine particles disappears: one can think that they coalesce to form larger particles.

Chemical composition analysis was carried out by inductive coupled plasma atomic emission spectroscopy (ICP-AES, Iris spectrometer, Thermo Fisher Scientific, Waltham, MA). Solutions were obtained by microwaves dissolution of glazes powders in an acids mixture. Injected within an argon plasma, their chemical elements are excited and emit characteristic radiations (UV and visible wavelengths) and hence can be identified and quantified.

Only the three principal oxides (oxides #1, #2, and #3) that play a relevant role on the softened glaze viscosity and its surface tension were titrated. Measured oxide losses (Table 7) are nearly the same than ICP-AES experimental error, which means that oxides were not vaporized nor decomposed when flame is sprayed (Table 7). With such results, one can deduce that initial glaze physical properties are not modified by flame treatment.

Table 7 Oxides relative losses (compared to as-received composition) according to heat treatment

	Oxide #1	Oxide #2	Oxide #3
After one flame treatment (densification)	−8 ± 5%	−7 ± 5%	−3 ± 5%
After two flame treatments (densification and spraying)	−10 ± 5%	−9 ± 5%	−8 ± 5%

5.2 Coating Structure

Figure 10 displays morphologies of coatings obtained with powders A, B, Y, and Z. Comparing coating

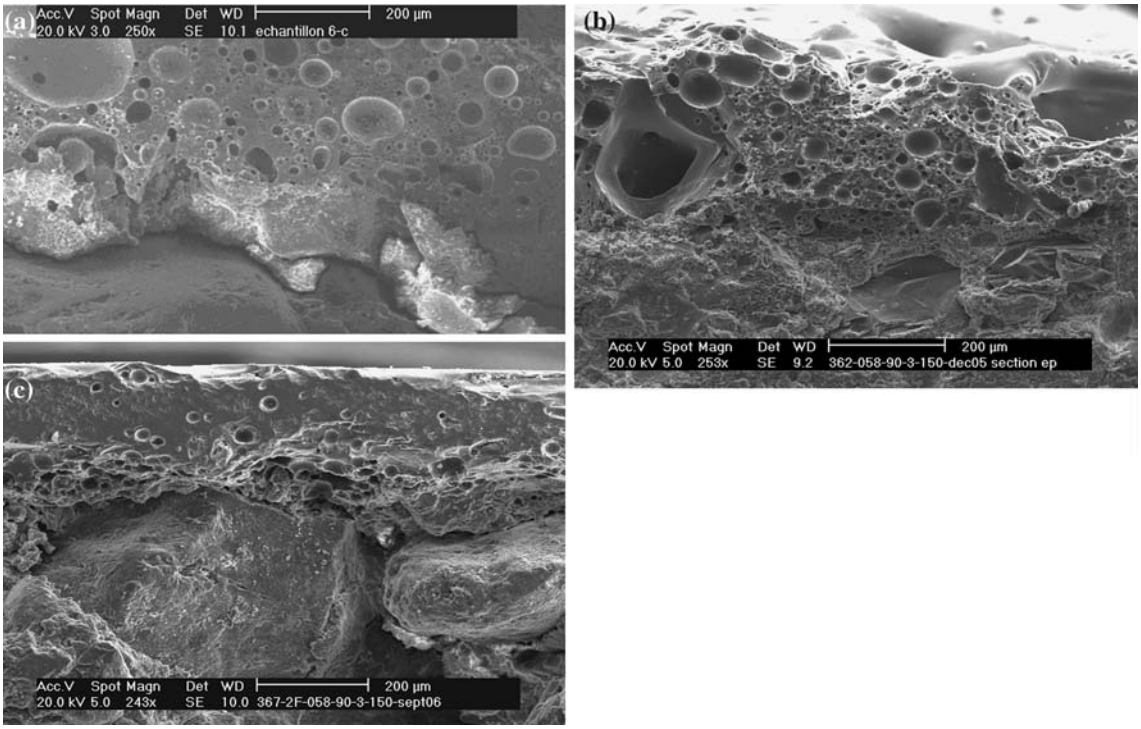

Fig. 11 Microstructure (SE-SEM) of a coating fracture (×250 magnification) obtained with (a) powder A, (b) powder B, and (c) powder Z

morphologies manufactured with agglomerated-sintered powders (Fig. 10a, b), one can say that unfused fine particles are visible on the surface coating realized with the high transition temperature feedstock A. In Fig. 10(b), an incomplete spreading of the particles is noticeable. Such a behavior is likely due to a feed rate too high, in regard with the kinematics of the torch. In turn, due to the cooling of the layer and consequently the increase in the glaze viscosity, particles impinging onto the surface do not coalesce anymore with the ones already deposited. According to Fig. 10(c), a low transition temperature glaze is not adapted to the process: cracks caused by stressed relief appear everywhere on the surface coating.

There is no visible or evident sign of a poor adhesion between the coating and the substrate (Fig. 11), whatever be the feedstock powder composition (and hence the transition temperature).

Figure 10(a) and (b) shows that feedstock flame pretreatment positively influences coating morphology. Indeed, coatings manufactured with agglomerated-sintered and flame-densified powder (Fig. 10d) exhibit higher molten particle coalescence. It can be explained by the fact that particles of powder B treated by flame are denser than particles of as-received powder B. Consequently, the coating architecture displayed in Fig. 10(d) exhibits a more regular surface, with less porosity. On the contrary, coatings manufactured with angular feedstock present a rough surface (Fig. 10e), with fine unfused particles dispersed along the surface.

One critical point is to prevent the substrate from thermal degradation (such a substrate risks decomposition by binder vaporization (Ref 11)). Furthermore, as it presents a low thermal conductivity, heat from flame and softened particles accumulate on the surface substrate (this phenomenon still has to be fully quantified by experimental measurements). Nevertheless, no severe substrate degradation was ever observed at the coating-substrate interface or close to the interface, meanwhile different glazes compositions corresponding to different heat releases (and with constant operating parameters and for an identical substrate) were tested. From samples observations and for the considered operating parameters, one can hence conclude that tested glazes compositions' spraying induces no visible substrate degradation. It can be explained in a first approximation, by the fact that glazes compositions are relatively identical, and so the particles' average temperatures upon impact are very likely the same for constant operating parameters. One can hence consider that the morphology differences observed on coatings surfaces obtained from different glazes compositions are primarily due to differences of viscosity and surface tensions of softened glazes rather than significantly different thermal heat transfers.'

6. Conclusions

It is possible to manufacture glaze layers by flame spraying onto substrates that decompose when heated and for which the traditional glazing process is not appropriate.

This preliminary study permitted to highlight the major effects of the operating parameters. The coating results

from one pass in front of the surface to be covered. The layers are almost crack-free and globular pores develop, very likely, due to the coalescence of the pores initially present within the powder particles.

The feedstock composition and morphology play relevant role in the coating structure. Adjusting the chemical composition permits to adjust the transition temperature of the materials. Adjusting their morphology by post-treatment permits to increase the deposition efficiency and to reduce the pore content of the coatings.

No visible delamination at the substrate-coating interface was ever detected in spite of the development of globular pores.

Complementary works will aim at quantifying the possible decomposition of glazes upon spraying as well as some of their functional properties.

Acknowledgments

This study was supported by the *Association pour le Développement et la Promotion du Pôle Européen de la Céramique*, Limoges, France, under Grant Number 05 005435/01/02. Its support is gratefully acknowledged by the authors.

References

1. G. Aliprandi, *Materiaux réfractaires et céramiques techniques – ingénierie des céramiques* (Refractory Materials and Technical Ceramics – Ceramics Engineering), Septima Edition, Paris, France, 1979, p 211-236, in French
2. T. Haure, ''Couches multi-fonctionnelles élaborées par plusieurs techniques'' (Multifunctional Layers by Multitechnique Process), Ph.D. Thesis, Faculty of Sciences, University of Limoges, France, 2003, in French
3. J.C. Labbe, E.N. Labrador, P. Lefort, and V. Leroux, Etude de la mouillabilité de l'INVAR par un émail (Study of the INVAR Wettability by an Enamel), *Ann. Chim. Sci. Mater.*, 2000, **25**, p 495-507, in French
4. E. Lugsheider, P. Remer, A. Nyland, and R. Sicking, Thermal Spraying of Bioactive Glass Ceramics, *Thermal Spray Science & Technology*, C.C. Berndt and S. Sampath, Ed., ASM International, Materials Park, OH, 1995, p 583-587, in French
5. J. Disam, K. Lübbers, U. Neudert, and A. Sickinger, Effect of Spraying Parameters of the LPPS Method on the Structure of Ceramics Coatings. Thermal Spray: Research, Design and Applications, C.C. Berndt and T.F. Bernecki, Eds., Materials Park, OH: ASM International, 1993, p 487-491
6. T. Zhang, Z. Qiu, Y. Bao, D.T. Gawne, and K. Zhang, Temperature Profiles and Thermal Stress Analysis of Plasma Sprayed Glass-Composite Coatings. Thermal Spray: Surface Engineering via Applied Research, C.C. Berndt, Ed., Materials Park, OH: ASM International, 2000, p 355-361
7. P. Chraska, V. Brozek, B.J. Kolman, J. Ilavsky, K. Neufuss, J. Dubsky, and K. Volenik, Porosity Control of Thermally Sprayed Ceramics Deposits. Thermal Spray: Meeting the Challenges of the 21st Century, C. Coddet, Ed., Materials Park, OH: ASM International, 1998, p 1299-1304
8. Y. Bao, T. Zhang, and D.T. Gawne, Analysis of Residual Stresses Generated During Plasma Spraying of Glass Coatings. Thermal Spray: Meeting the Challenges of the 21st Century, C. Coddet, Ed., Materials Park, OH: ASM International, 1998, p 575-580
9. T. Poirier, ''Dépôts de zircone colloïdale sur des substrats métalliques par projection à la flame d'aérosol'' (Colloidal Zirconia Coating on Metallic Substrates by Acrosol Flame Spraying), Ph.D. Thesis, Faculty of Sciences, University of Limoges, France, 2000, in French
10. A. Proner, ''Revêtements par projection thermique'' (Coatings by Thermal Spraying), Techniques de l'Ingénieur, M1645, p 11-12, in French
11. A. Saakov, Yu. Borisov, K. Yushchenko, and G. Komsky, Protective-Decorative Plasma Coatings on Concrete Structures, *Thermische Spritzkonferenz*, Ed. DVS, German Welding Society, Düsseldorf, Germany, 1993, p 212-215
12. P.-G. de Gennes, Gouttes, bulles, perles et ondes (Drops, Bubbles, Pearls and Waves), Belin edition, Paris, France, 2002, p 252, in French